Chemical Engineering Journal 499 (2024) 156165

Contents lists available at ScienceDirect

Chemical Engineering Journal

journal homepage: www.elsevier.com/locate/cej

Properties of cement raw meals used as sorbents in a calcium looping process

José Aguirre Castillo [a,b,c,*], Bodil Wilhelmsson [a,b,c,d], Markus Broström [a,b], Matias Eriksson [a,b,d]

[a] Centre for Sustainable Cement and Quicklime Production, Department of Applied Physics and Electronics, Umeå University, SE-907 87 Umeå, Sweden
[b] Thermochemical Energy Conversion Laboratory, Department of Applied Physics and Electronics, Umeå University, SE 901 87 Umeå, Sweden
[c] Heidelberg Materials Cement Sverige AB, SE-100 74 Stockholm, Sweden
[d] Swedish Mineral Processing Research Association – MinFo, SE-100 44 Stockholm, Sweden

ARTICLE INFO

Keywords:
Cement raw meal
Cement clinker
Carbon capture
Calcium looping

ABSTRACT

Calcium looping (CaL) is a promising carbon capture and storage (CCS) technology that has the potential to significantly reduce CO_2 emissions in cement production. Integrating CaL with cement production provides a viable solution to the high CO_2 emissions generated during the calcination process. This study examines the behavior of two industrial cement raw meals from different sites (A-RM and B-RM) under CaL conditions, focusing on phase composition, particle size distribution, and clinker phase evolution up to 1450 °C. Calcination and CaL experiments were conducted in a CO_2-rich atmosphere, with materials characterized using quantitative X-ray diffraction (Q-XRD) and high-temperature X-ray diffraction (HT-XRD). The results showed that both raw meals absorbed similar amounts of CO_2 during the cyclic CaL experiments. A-RM formed C_2S and other silicates, while B-RM retained more free CaO due to a less effective reaction with coarser quartz (SiO_2) particles. HT-XRD revealed delayed clinker-phase evolution in the 1000–1400 °C range in CaL-treated raw meals. However, CaL-treated raw meals achieved low free CaO at 1450 °C, suggesting that optimal kiln conditions can produce the desired phase composition. These findings indicate that integrating CaL-treated raw meals into cement production requires careful optimization of operational parameters to maintain clinker quality and minimize energy consumption. Further research should focus on improving the efficiency and reactivity of CaL-treated raw meals to enhance their suitability for industrial cement production.

1. Introduction

Cement production is responsible for approximately 8 % of global CO_2 emissions, with the calcination process alone accounting for roughly 60 % of that figure [1]. Cement raw meal, which is rich in $CaCO_3$, is calcined to produce free CaO, liberating CO_2 as a byproduct. Given the scale of the cement industry, this has a substantial impact on global greenhouse-gas concentrations. Efforts to reduce emissions have therefore focused on improving the efficiency of the cement manufacturing process and developing alternative methods that lower the carbon footprint of cement production.

One promising approach is the integration of calcium looping (CaL) technology, a carbon capture and storage (CCS) method that leverages the reversible reaction between CaO and CO_2 to capture and recycle emissions [2–4]. This study focuses on the properties of cement raw meals calcined in a high CO_2 atmosphere within the context of CaL, exploring how these conditions affect the material and its performance in subsequent clinker production. As illustrated in Fig. 1, CaL systems can be integrated into cement-kiln lines, where the necessary CaO exists in the raw meal used in cement production.

The CLEANKER project, for example, is a prominent demonstration of this integration, achieving a Technology Readiness Level (TRL) 7, but also highlighting challenges such as material recirculation and phase behavior that need to be addressed for wider adoption [1]. The project also explored the use of CaL-treated raw meals for clinker production. These raw meals were characterized and used to produce clinker in a

Abbreviations: CaL, calcium looping; CCS, carbon capture and storage; CCU, carbon capture and utilization; XRD, X-ray diffraction; Q-XRD, quantitative X-ray diffraction; HT-XRD, high temperature X-ray diffraction; XRF, X-ray fluorescence; HT, high-temperature; FWHM, full width at half maximum; C_3S, $3CaO•SiO_2$; C_2S, $2CaO•SiO_2$; C_3A, $3CaO•Al_2O_3$; C_4AF, $4CaO•Al_2O_3Fe_2O_3$; CS, $CaO•SiO_2$; CA, $CaO•Al_2O_3$.

* Corresponding author at: Umeå University, SE-907 87 Umeå, Sweden.
E-mail address: jose.aguirre@umu.se (J.A. Castillo).

https://doi.org/10.1016/j.cej.2024.156165
Received 15 August 2024; Received in revised form 23 September 2024; Accepted 24 September 2024
Available online 26 September 2024

laboratory setting, showing good burnability and confirming the potential to reintegrate these materials into the clinker production process. However, a lower C_3S/C_2S-ratio ratio was observed in the clinker produced from the looped meals, attributed to calcium depletion during the CaL process [5]. This observation underscores the need for optimization, high-quality materials, and advanced characterization methods to fairly evaluate the suitability of CaL-treated materials in cement production.

Studies on the calcination of cement raw meals in CO_2-rich atmosphere have shown that CO_2-liberation temperatures shift to higher levels due to changes in chemical equilibrium [6]. Calcite ($CaCO_3$), the primary carbonate in cement raw meals, decomposes during calcination to form calcium oxide (CaO) and CO_2. This process is influenced by the physical properties of calcite—such as surface texture, porosity, crystallite size, and particle size—which are critical factors affecting CO_2 liberation efficiency [7,8]. Additionally, calcite's thermal stability, impurity content, and interaction with other raw meal components like clay minerals and silica further impact its decomposition [9,10]. Operational parameters such as temperature, heating rate, and calcination atmosphere also play significant roles in the efficiency of this process.

Once formed, CaO plays a crucial role in both capturing CO_2 during the carbonation phase and reacting with other oxides in the raw meal, which influences the formation of key clinker phases, such as C_3S ($3CaO{\bullet}SiO_2$), C_2S ($2CaO{\bullet}SiO_2$), C_3A ($3CaO{\bullet}Al_2O_3$) and C_4AF ($4CaO{\bullet}Al_2O_3Fe2O_3$). Clinkers produced in high-CO_2 atmosphere exhibit larger crystal sizes of these phases, which leads to poorer reactivity compared to clinkers formed in low-CO_2 conditions [11].

Furthermore, the efficiency of CaL as a CCS technology depends on the properties of CaO, including its particle size, chemistry, and the conditions under which it is formed and cycled [12,13]. Repeated CaL cycles reduce the porosity and surface area of CaO, diminishing its ability to absorb CO_2 [13–15]. The formation of a thin $CaCO_3$ layer on CaO particles during CO_2 absorption further slows the process, while higher calcination temperatures can cause CaO sintering, reducing its reactivity and negatively impacting the overall efficiency of the CaL process [6,12,16].

Moreover, the formation of new species such as C_2S during CaL further complicates the process, as these species can decrease the efficiency of CO_2 absorption. C_2S typically forms at temperatures around 800 °C in CaL conditions, although formation at 700 °C has been reported in other contexts [17–24]. Accurately quantifying the impact of C_2S on CO_2 absorption remains challenging, with conventional methods potentially overestimating its presence. Advanced techniques like in-situ high-temperature X-ray diffraction (HT-XRD) are essential for gaining deeper insights into these phase evolutions, which are critical for optimizing the integration of CaL into cement production [25].

The kinetics behind the formation of compounds during the CaL process have been previously studied, but the reactivity of the spent raw meal from CaL in a cement kiln has not. This study aimed to investigate the properties of cement raw meal that had been thermally treated, as in a CaL process. We examined the phase composition, assessed whether new species agglomerated or grew in particle size, and, for the first time, evaluated the evolution of clinker phases using HT-XRD to understand how CaL affects clinker formation. This approach facilitated exploration of the feasibility of the use of CaL-processed raw meals in cement-clinker production.

2. Materials

Two industrial raw meals were chosen to represent different behaviors during the formation of clinker phases, as presented in our previous works [25]. Raw meal A (A-RM) has previously been shown to have a rapid combination of free CaO into clinker minerals. At 1000 °C, in both in-situ and ex-situ conditions, it was found that A-RM may contain up to 30 wt% free CaO. In contrast, raw meal B (B-RM) was chosen because of a slow free CaO combination. It has been found that B-RM may contain up to 60 % unreacted free CaO when calcined at 1000 °C [25]. Theoretically, if more free CaO is available, more CO_2 can be absorbed; thus, B-RM should be more efficient than A-RM in CaL applications. The oxide chemistry and sieve residues of A-RM and B-RM, obtained using XRF and laser diffraction, respectively, are shown in Table 1.

The differences in reactivity between the two raw meals were primarily related to the fineness of their components [25]. For example, B-RM contained more quartz (SiO_2) of coarseness greater than 45 μm, which inhibits the formation of clinker minerals, resulting in clusters of C_2S in the clinker [25,26].

Table 2 shows the phase composition of both A-RM and B-RM, as determined by Q-XRD. Some phases have been grouped according tTable 1o their mineral families.

3. Methods

3.1. Chemical analysis and particle-size distribution

The elemental composition of the untreated raw-meal samples shown in was obtained using XRF analysis with a Panalytical Axios XRF instrument (Malvern Panalytical, UK) and carbon and sulfur analysis with a LECO CS 230 instrument (LECO, US).

An overview of the material fineness in terms of particle-size distribution was obtained using laser diffraction with a Malvern Mastersizer

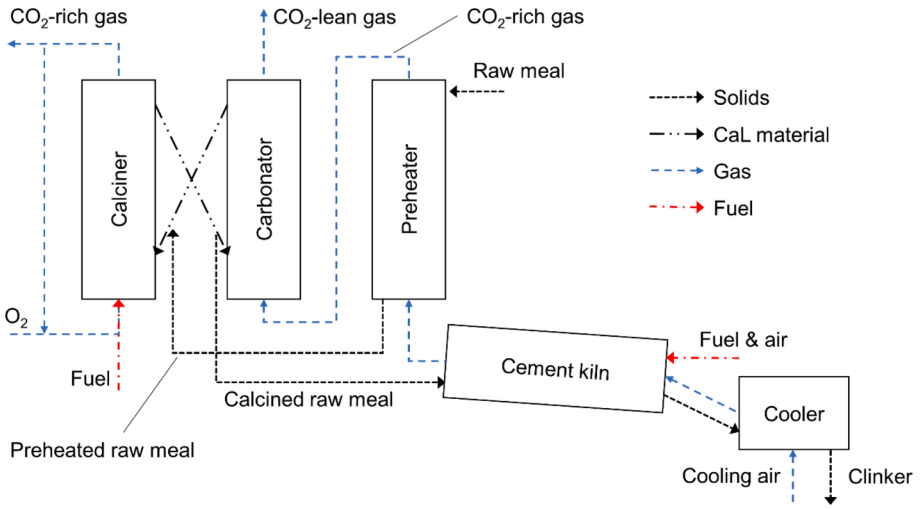

Fig. 1. Schematic diagram of a calcium-looping system integrated in the production of cement clinker.

Table 1
Chemical composition (determined by XRF and carbon and sulfur analysis) of A-RM and B-RM, expressed as oxides and sieve residues (wt%).

	CaO	SiO_2	Al_2O_3	Fe_2O_3	MgO	K_2O	Na_2O	SO_3	CO_2	>90 μm	>200 μm
A-RM	42.9	13.1	3.36	1.89	2.85	0.82	0.22	1.07	34.6	15.9	1.5
B-RM	43.1	13.7	3.41	1.67	1.37	0.59	0.44	0.85	37	10.7	2.5

Table 2
Phase composition of A-RM and B-RM, as determined by Q-XRD.

	Calcite	Quartz	Dolomite	Åkermanite	Pyroxenes	Feldspars	Micas	Phyllosilicates	Other
A-RM	69.3	8.9	8.4	2.8	1.9	3.2	3.5	1.5	0.4
RM-B	77.3	5.7	–	0.2	3.6	5.5	1.8	4.5	1.4

3000 (Malvern Panalytical, UK) with water dispersion. After heat treatment, the materials were analyzed after being dispersed in ethanol.

3.2. Q-XRD, HT-XRD, and the Rietveld method

The phase compositions of the raw meals before and after heat treatment were obtained using XRD with a Panalytical X'Pert (Malvern Panalytical, UK) with Bragg-Brentano geometry and Cu-Kα radiation (λ = 1.5408 Å) at 45 kV and 40 mA. The 10° to 65° 2θ angular window was investigated using a silicon strip detector with a step size of 0.02 °2θ and 200 s/step.

The samples were mounted using a Panalytical back-loading device (Malvern Panalytical, UK). Some of the agglomerated samples required gentle milling with a mortar and pestle. The milling was conducted such that the effect on the particle size was minimized. The coarse fraction of each sample was measured with powder XRD after sieving with a 45 μm sieve and an electric sieve shaker, both from Retsch (Retsch GmbH, DE).

The DIFFAC.TOPAS 6.0 software (Bruker AXS GmbH, DE) was used for phase quantification (Q-XRD), together with structure files from the Inorganic Crystal Structure Database (ICSD). The structure files used are listed in Table S 1 in Appendix 1. The Rietveld method was used for the Q-XRD to refine the theoretical model to fit the observed XRD data. The structure files for the phases were refined for scale factors, cell parameters, peak broadening, and strain. At the same time, a background function was fitted along with other parameters, such as specimen displacement and peak shapes. Fig. 2 shows the observed intensities, I_{obs}, and calculated intensities, I_{calc}, of Sample A-RM-1L. The major phases in A-RM-1L (presented later) are displayed in Fig. 2, showing their contribution to I_{calc}.

The phase evolution and formation of clinker phases were studied using HT-XRD, for which the previously mentioned XRD instrument was equipped with an Anton Paar HTK 2000 N high-temperature (HT) chamber (Anton Paar GmbH, AT). Before the HT measurements, six grams of each sample was slightly milled using a Retsch MM 400 ball mill (Retsch GmbH, DE) with 25 ml ZrO jars and 20 mm milling balls for 1 min at 30 Hz. The samples were then mounted on the platinum heating strip inside the HT chamber. Care was taken to achieve an area of 10 × 10 mm and thickness of <0.5 mm, as recommended by the manufacturer. The platinum heating strip was heated at 10 °C/min. XRD measurements were collected at 1000, 1100, 1200, 1300, 1350, 1400, and 1450 °C, with a holding time of 5 min before collection. Cooling occurred at 400 °C/min down to 1000 °C, then at 200 °C/min down to 25 °C. A final measurement of the cooled sample was collected. Data collection was done within 10° and 65° 2θ, with a step size of 0.02 °2θ and 50 s/step.

4. Production of calcined and carbonated raw meals

A Nabertherm muffle furnace with scale (Nabertherm GmbH, DE) and installed gas supply (Voegtlin Instruments GmbH, CH) were used to produce calcined raw meals and simulate CaL conditions. The samples were contained in platinum bowls with a diameter of roughly 3 cm. Each test used 30 g of sample dispersed across four bowls to ensure good contact between the samples and the gas inside the furnace.

The furnace, which had a volume of 9 L, was supplied with gas at 3 L/min. A reference calcination at 950 °C was conducted with a 100 vol% N_2 atmosphere for A-RM and B-RM, resulting in samples A-RM-N2 and B-RM-N2. A second calcination at 950 °C was conducted with 80 vol% CO_2 in N_2, resulting in samples A-RM-CO2 and B-RM-CO2. The cooling following both calcination tests was carried out in N_2. The weight of the samples was tracked using the integrated scale.

The one-loop CaL experiment was carried out as follows:

1. Temperature increase at 10 °C/min up to 950 °C, with 80 vol% CO_2 in N_2
2. 20 Min holding time at 950 °C with 80 vol% CO_2 in N_2

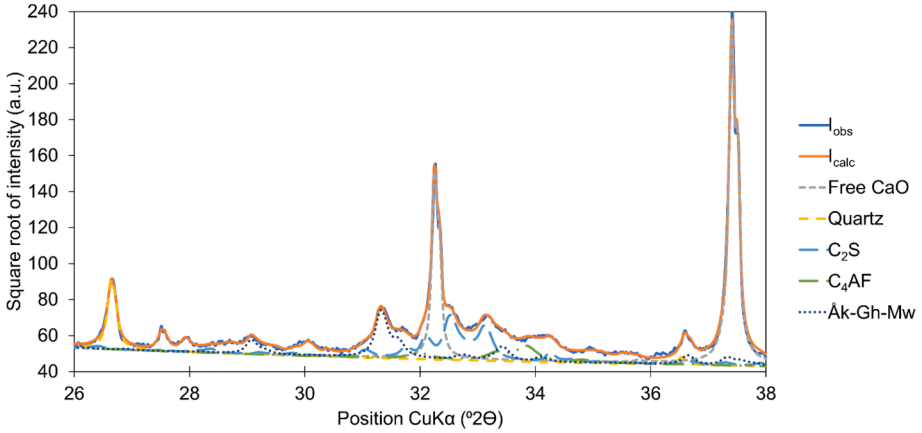

Fig. 2. Q-XRD data for Sample A-RM-1L. Curve Åk-Gh-Mw shows the summed intensity of the Åkermanite, Gehlenite, and Merwinite phases.

3. Cooling at 5 °C/min to 650 °C with 20 vol% CO_2 in N_2
4. 20 Min holding time at 650 °C with 20 vol% CO_2 in N_2
5. Temperature increase at 10 °C/min up to 950 °C with 80 vol% CO_2 in N_2
6. 20 Min holding time at 950 °C with 80 vol% CO_2 in N_2 (Loop 1 complete)
7. Cooling to room temperature in N_2

For the three- and five-loop experiments, Steps 3–6 were repeated accordingly. The looped samples were designated A-RM-1L, A-RM-3L, and A-RM-5L for A-RM; and B-RM-1L, B-RM-3L, and B-RM-5L for B-RM. As with the calcination tests, the gas supply was 3 L/min, and the weight was logged with the integrated scale.

Extra samples of A-RM were produced. The first sample followed the A-RM-1L procedure but was cooled in N_2 after Step 4, and designated A-RM-Carb. The second sample, A-RM-CarbMax, also followed the procedure for A-RM-1L, but after Step 4 the temperature was increased to 820 °C (20 vol% CO_2 in N_2). A-RM-CarbMax rested at 820 °C for 60 min, then was cooled in N_2.

5. Results and discussion

5.1. Calcination tests

The temperature profile and weight evolution of the samples used in the calcination tests are presented in Fig. 3. The weight curves show that in 80 vol% CO_2, a higher temperature was required to initiate calcination for both raw meals. The weight of A-RM-N2 decreased slowly after 540 °C was reached, then quickly increased as the temperature approached 700 °C and attained a steady state at 950 °C. The calcination of A-RM-CO_2 took place in three steps: [1] the decomposition of dolomite ($CaMg(CO_3)_2$) between 550 and 750 °C, and some decomposition of phyllosilicates; [2] low rate decarbonization of calcite ($CaCO_3$) between 750 and 850 °C; [3] accelerated decarbonization of calcite from 850 °C onwards. The final weight of A-RM-N2 (65 wt%) and A-RM-CO2 (66 wt%) differed by only 1 wt%.

Table 3 presents the phase composition obtained using Q-XRD, showing minor differences between the two groups of samples, such as differences in consumed free CaO_{eq} and formed C_2S. Free CaO_{eq} was calculated using (1), assuming that portlandite ($Ca(OH)_2$) was formed from free CaO and atmospheric moisture (H_2O) during sample preparation and XRD measurement.

$$\text{Free } CaO_{eq} = \text{free CaO} + \text{portlandite} * (56/74) \quad (1)$$

The calcined B-RM samples had some similarities to the calcined A-RM samples. As can be seen in Fig. 3, B-RM-N2 started to lose weight at about 630 °C, with this loss accelerating as the temperature approached 700 °C. The weight loss of B-RM-CO2 started at approximately 690 °C, and accelerated at close to 850 °C. B-RM-CO2 started to lose weight at around 700 °C, and this accelerated at just past 800 °C. The acceleration of calcite decomposition was similar across the raw meals but the initial weight loss was not, which may have been caused by the different particle-size distributions (shown in Fig. 4). The accumulated percentage of particles below 15 μm was 43.3 % for A-RM and 30 % for B-RM.

The final weight of Sample B-RM-N2 was 63 wt%, while that of B-RM-CO2 was 7 wt% higher. Q-XRD results (Table 3) show that B-RM-CO2 contained about 4.5 wt% Spurrite ($Ca_5(SiO_4)_2CO_3$), which formed during the reaction of free CaO, quartz (SiO_2) and absorbed CO_2 [27]. Additionally, no C_3S formation was detected for the B-RM samples,

Table 3
Q-XRD results (wt%) from the calcination tests. "Other" includes phases such as feldspars, micas, and minor clinker phases.

	A-RM-N2	A-RM-CO2	B-RM-N2	B-RM-CO2
Free CaOeq	45.0	46.7	60.8	54.0
Calcite	0.1	0.1	0.5	0.4
Quartz	7.5	7.5	8.2	13.5
C_3S	1.4	1.4	–	–
C_2S	13.4	12.3	2.4	1.9
CS	–	–	2.4	1.6
C_3A	1.1	1.0	0.7	0.4
C_4AF	5.4	6.2	2.5	2.8
CA	2.4	2.6	–	–
Åk-Gh-Mw	13.4	14.1	4.1	2.9
Spurrite	3.1	3.2	2.8	4.5
Anhydrite	–	–	2.2	1.4
Other	7.5	5.9	13.5	17.8

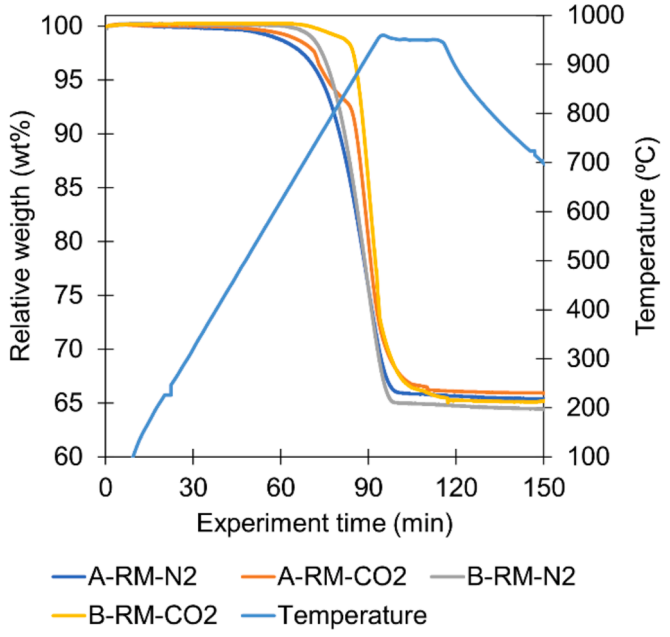

Fig. 3. Weight curves for calcination experiments with A-RM and B-RM. Weights are given as relative weights due to minor differences in the initial weights. The temperature profiles underwent minor disturbances during the data collection.

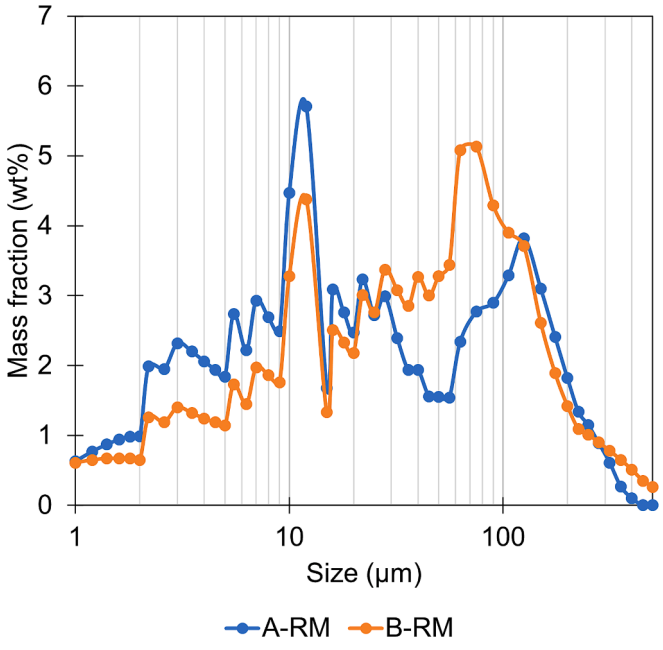

Fig. 4. The particle-size distribution of Samples A-RM and B-RM, obtained using laser diffraction and expressed as mass fraction.

although wollastonite ($CaO•SiO_2$, CS) was found.

5.2. Evaluation of calcium looping using Q-XRD

The CaL experiments produced the weight curves shown in Fig. 5. Only the five-loop (5L) weight curves are shown; the one-loop (1L) and three-loop (3L) sampling are marked at the corresponding experiment times. The following discussion will refer to the experiment time (t) in minutes so that it is easy to follow in Fig. 5.

Similar to the curves shown in Fig. 3, both raw meals that were calcined in 80 vol% CO_2 showed a stepwise weight loss at the beginning of the experiment, with A-RM and B-RM exhibiting 34 wt% and 30 wt% weight loss, respectively, at t = 110. After the first calcination step, cooling down to 650 °C was conducted in 20 vol% CO_2. Both materials started to gain weight at a high rate at temperatures below 780 °C (t ≈ 140) due to the absorption of CO_2. This absorption decelerated below 700 °C (t ≈ 160). After the 20-minute holding time at 650 °C (t = 180), the relative weights of A-RM and B-RM had increased by 72 wt% and 71 wt%, respectively.

Over time/loops, the distinctive weight gain (between t = 140 and 200) due to CO_2 absorption decreased. The Q-XRD results in Table 4 show that the silicates Åkermanite ($Ca_2Mg(Si_2O_7)$), Gehlenite ($Ca_2Al(AlSiO_7)$), and Merwinite ($Ca_3Mg(SiO_4)_2$) increased in A-RM while quartz and free CaO decreased, indicating that some of the reduction in CO_2 absorption capability over several loops can be credited to the formation of silicates other than C_2S. Similar trends were seen in the Q-XRD results (Table 4) for B-RM, although here feldspar and Spurrite were also consumed, and more C_2S was formed over an increasing number of loops.

The results show that although B-RM contained 54 wt% free CaO_{eq} after calcination in CO_2 (t = 110), its weight was ultimately the same as that of A-RM (absorbed CO_2 at t = 180), which had 46.7 wt% free CaO_{eq}. Previous studies have reported that a substantial amount of C_2S is formed during calcination in CO_2, meaning that less free CaO is available for CO_2 absorption [17–19]. Q-XRD results for A-RM-Carb show that at t = 180, the A-RM samples had no more than 14 wt% C_2S (Table 4). Table 4 also presents results from the A-RM-1L, −3L, and −5L experiments, where the amount of C_2S also did not exceed 13–14 %. Thus, the formation of C_2S is not a major hindrance to the CO_2 absorption of free CaO to the extent previously observed. It is likely that there is a limit to how much CO_2 can be absorbed in stationary experiments with limited mixing between fine powder particles, which prevents effective absorption. It is well known that calcination in a high-CO_2 atmosphere results in a sintered CaO surface that absorbs CO_2 less effectively [28]. Additionally, the solid diffusion of CO_2 through a thin layer of newly formed $CaCO_3$ on free CaO surfaces slows the absorption process [15].

Table 4
Q-XRD results for the looping experiments (wt%).

	A-RM					B-RM		
	1L	3L	5L	Carb	Carb Max	1L	3L	5L
Free CaOeq	45.5	46.2	44.5	32.7	6.4	56.3	53.5	55.5
Calcite	0.1	0.2	0.3	17.5	49.6	0.6	0.5	0.6
Quartz	6.5	5.4	4.4	7.4	5.1	11.4	12.5	11.3
C3S	1.5	2.3	2.3	0.0	0.5	–	–	–
C2S	13.6	13.0	13.8	14.0	12.4	2.2	3.1	3.6
CS	–	–	–	–	–	1.6	1.5	0.7
C3A	1.2	0.6	0.6	1.8	2.1	0.7	0.9	0.6
C4AF	6.0	5.1	5.7	4.0	3.8	3.9	3.3	4.0
CA	2.7	2.6	2.7	1.6	0.9	–	–	–
Åk-Gh-Mw	14.6	17.9	19.5	13.2	11.7	3.8	5.0	5.8
Spurrite	3.5	4.1	3.9	3.2	1.8	5.2	3.6	3.5
Anhydrite	–	–	–	–	–	1.3	1.5	1.6
Other	5.6	5.4	4.9	5.2	5.8	16.6	15.8	15.0
$L_{Free\ CaO}$ (nm)	135	129	130	60	36	123	147	147

Fig. 6 compares the temperature profiles and heating curves of A-RM-1L, A-RM-Carb, and A-RM-CarbMax. The Q-XRD results (Table 4) for A-RM-CarbMax show a calcite content of 49.6 wt% and free CaO_{eq} of 56 wt%, showing that further absorption of CO_2 is possible. However, the raw meal needs to be heated to a temperature close to calcination conditions in order for this to be achieved, which may not be practical in a full-scale process.

In previous studies, structural changes in free CaO have been reported based on the calculated crystallite size of the free CaO phase, which itself was calculated using XRD data [3,20,21]. In the present study, crystallite sizes were calculated according to the Scherrer equation (2). The obtained free CaO crystallite size, $L_{Free\ CaO}$, for each sample is shown in Table 4. In the Scherrer equation, β_{FWHM} is the full width at half maximum (FWHM) of the strongest free CaO peak (37.1° 2θ), θ is the Bragg angle, λ the wavelength, and k is the shape factor (0.94 for cubic crystallites). The crystallite sizes of A-RM and B-RM changed slightly between loops. It has been reported that increases in crystallite size can be caused by increases in CO_2 partial pressure [29] and calcination temperature [20]. The B-RM samples did not show any significant variation in crystallite size; among the A-RM samples, only the carbonated ones showed a lower crystallite size, a sign of higher disorder in the crystal structure of the free CaO.

$$L = k^{*}\lambda^{*}(\beta_{FWHM}{}^{*}\cos\theta)^{-1} \quad (2)$$

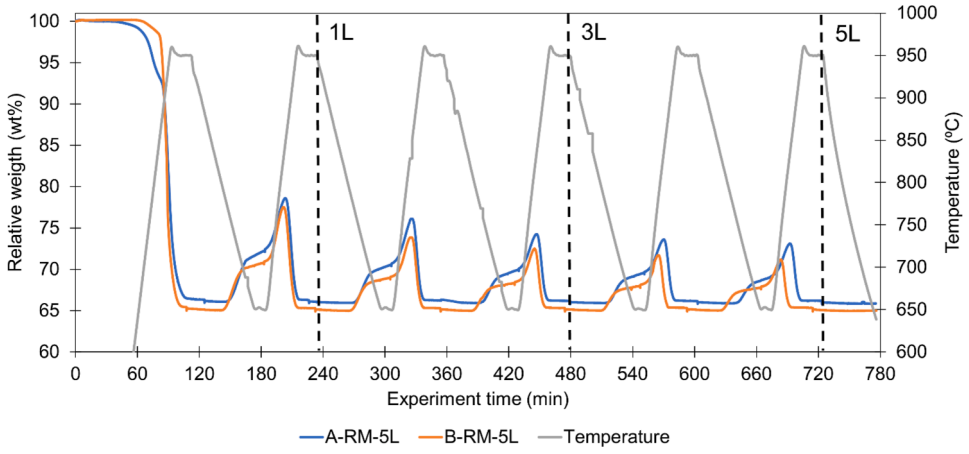

Fig. 5. Weight curves for the five-loop CaL experiment. The temperature profiles of both samples are overlayed. Disturbance in the data logging caused jagged curves.

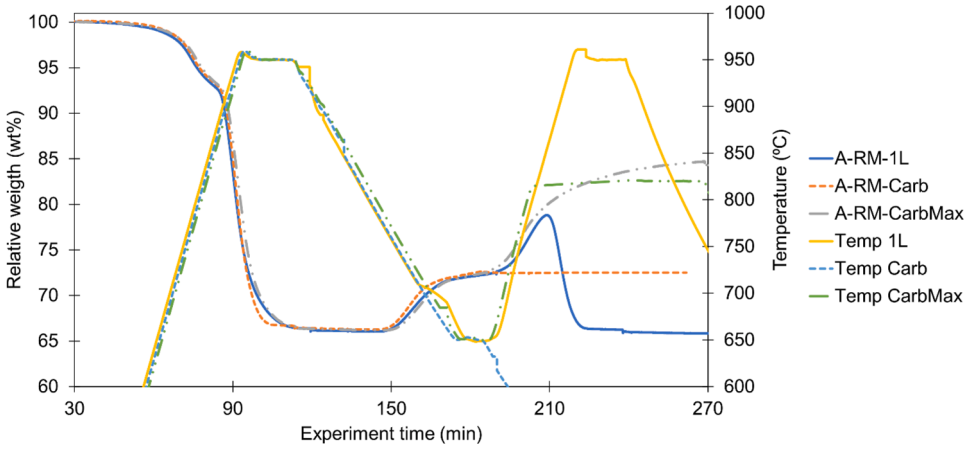

Fig. 6. Comparison of the A-RM-1L, A-RM-Carb, and A-RM-CarbMax weight curves.

5.3. The coarse fraction of CaL material

The particle sizes of the raw meals before and after looping are shown in Fig. 7. For both raw meals, particles below 10 μm decreased, while coarser particles above 30 μm increased. The coarse fraction of each sample was studied using a 45 μm sieve and Q-XRD. 45 μm is a widely used size of sieve to determine the coarse fraction of silica sources in raw meals that can negatively affect the burning process in the cement kiln [30]. In the A-RM samples, it was found that free CaO was more concentrated in the >45 μm fraction, as shown in Fig. 8. C_2S was slightly lower in the coarse fraction, with no major changes with increasing loops. This finding suggests that the particles of <5 μm in the A-RM samples may have been finely ground calcite ($CaCO_3$) that, after calcination, were combined into C_2S or coarser free CaO. For the B-RM samples the findings were different, as the amount of free CaO in the >45 μm fraction was lower, while the amount of quartz was higher (Fig. 8). As already discussed in relation to the calcination experiments, coarse quartz limited the formation of new phases in B-RM.

5.4. Evaluation of clinker-phase evolution using HT-XRD

An evaluation of the A-RM, A-RM-CO2, A-RM-1L, and A-RM-3L samples using HT-XRD produced the results shown in Fig. 9. The free CaO in the raw meal (A-RM) was consumed at a higher rate with increasing temperature. The sample calcined in CO_2 and the CaL samples reached the same amount of free CaO as A-RM at 1450 °C. The target level of free CaO in an ordinary cement clinker is usually 1–2 wt% [22]. We state that a CaL-treated raw meal is likely to require a higher processing temperature, thereby increasing kiln energy consumption. Another option is an increased residence time in the kiln, which affects kiln output. Otherwise, the clinker quality may be negatively affected.

Looking further into what causes the slow consumption of free CaO and formation of clinker minerals, the HT-XRD results showed that A-RM had steady C_2S formation. At 1000 °C, A-RM had already formed 31.8 wt% C_2S, which continued to increase with consumption of free CaO and quartz. The rate of formation of new C_2S in the samples calcined in CO_2 was slow at 1000–1100 °C, but increased at 1200 °C. A comparison of the phase evolution of the raw meal (A-RM) and the A-RM-1L samples is shown in Fig. 10. The changes in free CaO particle size discussed above may have decreased the contact area between the free CaO, quartz, and previously formed C_2S. C_2S can also form around quartz particles, creating a protective layer, as seen in industrially produced clinker [31]. We hypothesize that some melt formation at 1200 °C helped to dissolve the C_2S that formed around the quartz particles. Unfortunately, this was not possible to confirm using HT-XRD, and would require the production of a larger quantity of CaL material and clinker such that evaluation could be undertaken using microscopy methods.

6. Conclusions

Two cement raw meals were calcined and treated in order to investigate the concept of calcium looping. The resulting materials were characterized using Q-XRD, laser diffraction, and coarse-fraction analysis, and the evolution of clinker phases was studied using in-situ HT-XRD to assess the effects of CaL.

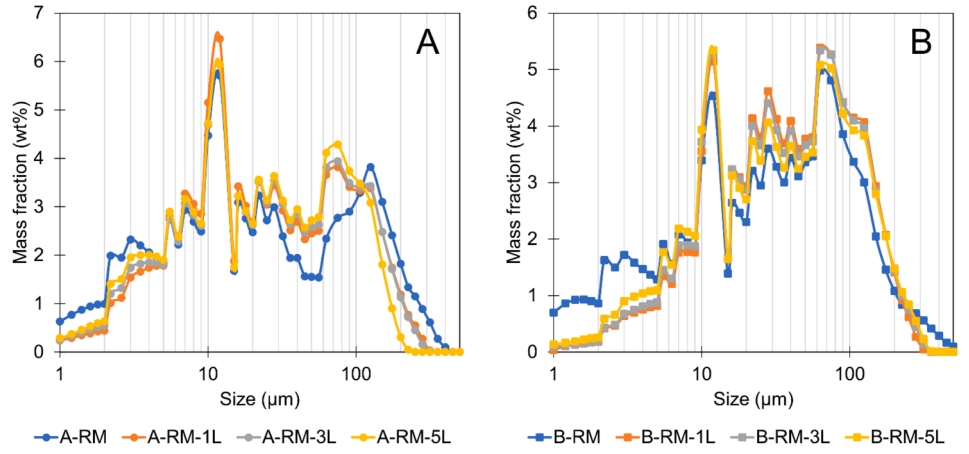

Fig. 7. Particle-size distribution, obtained using laser diffraction, of the raw meals and CaL samples of (A) A-RM and (B) B-RM.

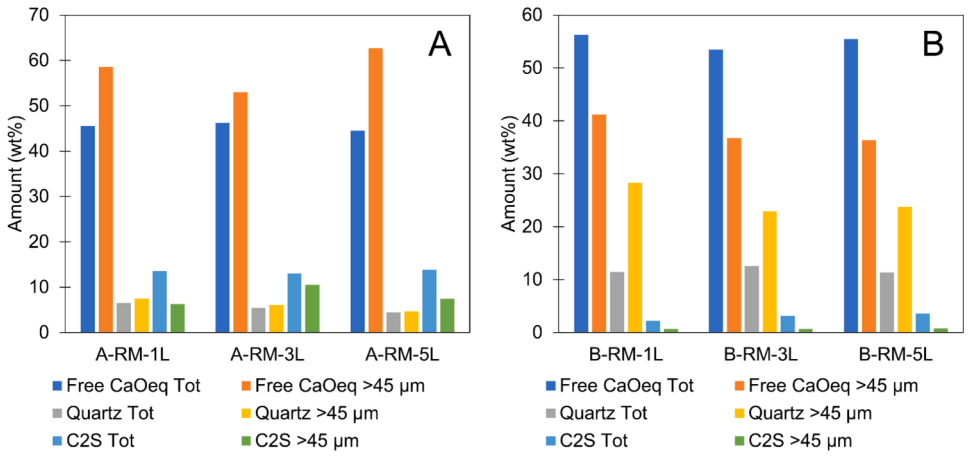

Fig. 8. Distribution of free CaO, quartz, and C_2S in the coarse fractions of (A) A-RM samples and (B) B-RM samples.

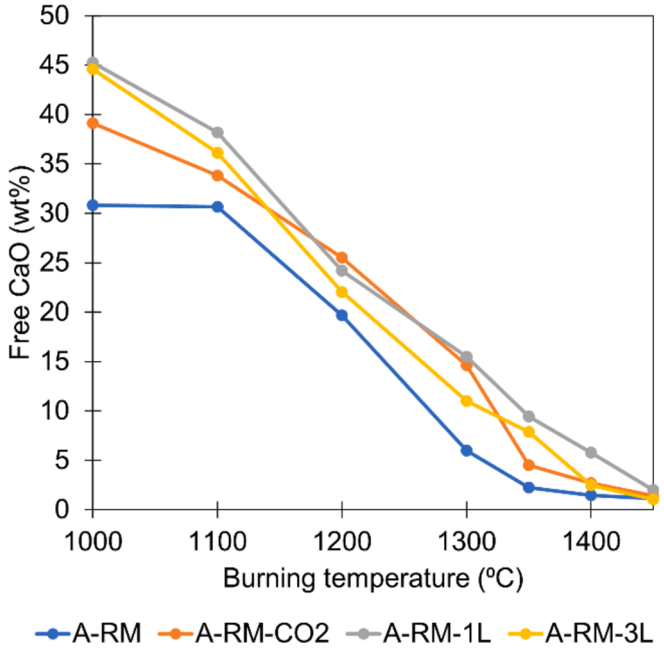

Fig. 9. HT-XRD (in-situ) measurement of the free CaO consumption in the A-RM samples.

The raw meals absorbed similar quantities of CO_2, despite A-RM having more free CaO available for CO_2 absorption after calcination in CO_2 than B-RM. This was attributed to insufficient mixing between gases and solids, along with changes in the microstructures of the CaO surfaces as the CO_2 absorption increased with temperature and residence time.

Particle-size distribution measurements and fractioning of the different samples helped to detect the consumption of finer particles and characterize newly formed ones. C_2S formed, and preexisting silicates grew. The results showed that C_2S formation is not a major limiting factor in the absorption of CO_2 by raw meals. The quantity of C_2S detected was not as large as in other studies. Quantification of C_2S using Q-XRD has challenges, but as has been shown here, it is useful and should also be undertaken in future studies.

The results imply that C_2S formed during CaL affects the reactivity of the raw meal by forming in a way that blocks further reactions with quartz. The HT-XRD testing showed that a CaL-treated raw meal has less reactivity, which may require more heat input or a longer residence time in the cement kiln.

Funding sources

The Swedish Energy Agency, grant number 50893-1 and 50224-1. Ellen, Walter, and Lennart Hesselman Foundation for Scientific Research, grant number 2023. Horizon Europe, grant number 101138392.

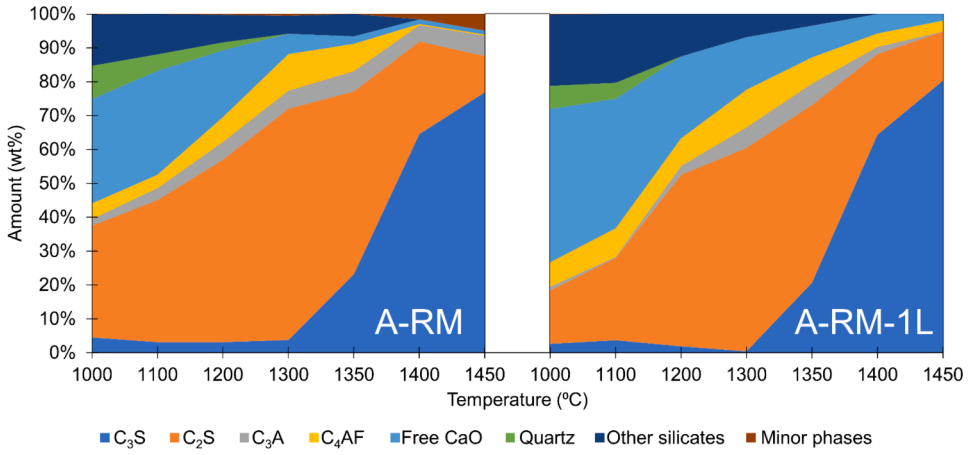

Fig. 10. Phase evolution of the A-RM and A-RM-1L samples, analyzed using (in-situ) HT-XRD.

8. Glossary

- Calcium Looping (CaL): A carbon capture and storage (CCS) technology that utilizes the reversible reaction between calcium carbonate ($CaCO_3$) and free CaO to capture and recycle CO_2 emissions during cement production.
- Calcination: The process of heating a substance to a high temperature in the presence of air or oxygen, causing thermal decomposition. In cement production, it refers to the heating of calcium carbonate ($CaCO_3$) to produce free CaO and liberate CO_2.
- Cement clinker: The solid material produced in the kiln during cement production, consisting mainly of C_3S, C_2S, C_3A, and C_4AF phases. It is ground to produce cement.
- Sintering: A process where particles of a material, such as CaO, coalesce and bond together when heated, leading to a reduction in porosity, increased density, and enhanced mechanical strength.
- Rietveld Method: A mathematical approach used in X-ray diffraction to refine the crystal structure model and quantify phase composition in a sample.

CRediT authorship contribution statement

José Aguirre Castillo: . **Bodil Wilhelmsson:** Writing – review & editing, Supervision, Project administration, Funding acquisition. **Markus Broström:** Writing – review & editing, Supervision, Project administration, Funding acquisition. **Matias Eriksson:** Writing – review & editing, Supervision, Project administration, Funding acquisition, Conceptualization.

Declaration of competing interest

The authors declare the following financial interests/personal relationships which may be considered as potential competing interests: Matias Eriksson reports financial support was provided by Ellen Walter and Lennart Hesselman Foundation for Scientific Research. Bodil Wilhelmsson reports financial support was provided by Swedish Energy Agency. Markus Brostrom reports financial support was provided by Horizon Europe. Bodil Wilhelmsson reports a relationship with Heidelberg Materials Cement Sverige AB that includes: board membership and employment. Jose Aguirre Castillo reports a relationship with Heidelberg Materials Sweden AB that includes: board membership and employment. If there are other authors, they declare that they have no known competing financial interests or personal relationships that could have appeared to influence the work reported in this paper.

Data availability

Data will be made available on request.

Acknowledgments

This work was performed within the Centre for Sustainable Cement and Quicklime Production at Umeå University, and partly funded by the Swedish Energy Agency, Hesselman Foundation and European Commission. Other collaborators mentioned in this work are Heidelberg Material Cement Sverige AB, SMA Mineral AB, and the Swedish Mineral Processing Research Association – MinFo.

Appendix A. Supplementary data

Supplementary data to this article can be found online at https://doi.org/10.1016/j.cej.2024.156165.

References

[1] M. Alain, Decarbonisation options for the cement industry, EUR 31378 EN, Publications Office of the European Union, Luxembourg, 2023.
[2] M.C. Romano, et al., The calcium looping process for low CO2 emission cement plants, Energy Procedia 61 (2014) 500–503.
[3] J.M. Valverde, P.E. Sanchez-Jimenez, L.A. Perez-Maqueda, On the relevant influence of limestone crystallinity on CO2 capture in the Ca-looping technology at realistic calcination conditions, Environ. Sci. Technol. 48 (no. 16) (2014) 9882.
[4] J. Blamey, et al., The calcium looping cycle for large-scale CO2 capture, Prog. Energy Combust. Sci. 36 (no. 2) (2010) 260.
[5] D. Gastaldi, et al., Clinker based on calcium looped meals from the Cleanker Project, J. Microsc. 294 (2) (2024) 90–104.
[6] J.R. Fernandez, S. Turrado, J.C. Abanades, Calcination kinetics of cement raw meals under various CO2 concentrations, React. Chem. Eng. 4 (12) (2019) 2129–2140.
[7] T. Darroudi, A.W. Searcy, Effect of carbon dioxide pressure on the rate of decomposition of calcite (CaCO3), J. Phys. Chem. 85 (26) (1981) 3971–3974.
[8] J. Khinast, et al., Decomposition of limestone: The influence of CO2 and particle size on the reaction rate, Chem. Eng. Sci. 51 (4) (1996) 623–634.
[9] K. Sandström, Effects of Impurities on Phase Equilibrium in Quicklime and Cement Clinker Production, Umeå University, Umeå, 2024, p. 76.
[10] D. Herfort, D.E. Macphee, *3 - Components in Portland Cement Clinker and Their Phase Relationships*, in *Lea's Chemistry of Cement and Concrete (Fifth Edition)*, P.C. Hewlett and M. Liska, Editors. 2019, Butterworth-Heinemann. p. 57-86.
[11] F. Ming, et al., *Research on the effect of CO2/O2 atmosphere on calcined cement clinker*, in *ZKG Cement Lime Gypsum Einzelheft*. 2023, ZKG Cement Lime Gypsum.
[12] R. Barker, The reversibility of the reaction CaCO3 ⇄ CaO+CO2, J. Appl. Chem. Biotech. 23 (10) (1973) 733–742.
[13] G.S. Grasa, J.C. Abanades, CO2 capture capacity of CaO in long series of carbonation/calcination cycles, Ind. Eng. Chem. Res. 45 (no. 26) (2006) 8846.
[14] G. Grasa, et al., Application of the random pore model to the carbonation cyclic reaction, AIChE J. 55 (no. 5) (2009) 1246.
[15] J.M. Valverde, A model on the CaO multicyclic conversion in the Ca-looping process, Chem. Eng. J. 228 (2013) 1195–1206.
[16] S. Chen, et al., Understanding sulfation effect on the kinetics of carbonation reaction in calcium looping for CO2 capture, Fuel Process. Technol. 221 (2021) 106913.
[17] M. Alonso, J.R. Fernández, J.C. Abanades, Kinetic study of belite formation in cement raw meals used in the calcium looping CO2 capture process, Ind. Eng. Chem. Res. 58 (14) (2019) 5445–5454.
[18] M. Alonso, et al., Characterization of a Marl-type cement raw meal as CO2 sorbent for calcium looping, ACS Omega 3 (11) (2018) 15229–15234.
[19] M. Alonso, et al., CO2 carrying capacities of cement raw meals in calcium looping systems, Energy Fuel 31 (12) (2017) 13955–13962.
[20] S.K. Pathi, et al., CO2 capture by cement raw meal, Energy Fuel 27 (9) (2013) 5397–5406.
[21] J. Plou, et al., Reactivity of calcined cement raw meals for carbonation, Powder Technol. 354 (2019) 338–347.
[22] P. del Strother, *2 – Manufacture of Portland Cement*, in *Lea's Chemistry of Cement and Concrete (Fifth Edition)*, P.C. Hewlett and M. Liska, Editors. 2019, Butterworth-Heinemann. p. 31-56.
[23] S. Telschow, et al., Cement formation: a success story in a black box: high temperature phase formation of portland cement clinker, Ind. Eng. Chem. Res. 51 (34) (2012) 10983–11004.
[24] E. Viggh, et al., Early formation of belite in cement clinker raw materials with slag, Adv. Cem. Res. 33 (6) (2021) 249–256.
[25] J. Aguirre Castillo, M. Broström, M. Eriksson, Phase evolution and burnability of cement raw meal, Adv. Cem. Res. 35 (12) (2023) 577–587.
[26] D.H. Campbell, *Microscopical Examination and Interpretation of Portland Cement and Clinker*. 1999: Portland Cement Association.
[27] H. Bolio-Arceo, F.P. Glasser, Formation of spurrite, Ca5(SiO4)2CO3, Cem. Concr. Res. 20 (2) (1990) 301–307.
[28] F. García-Labiano, et al., Calcination of calcium-based sorbents at pressure in a broad range of CO2 concentrations, Chem. Eng. Sci. 57 (13) (2002) 2381–2393.
[29] J.M. Valverde, P.E. Sanchez-Jimenez, L.A. Perez-Maqueda, Limestone calcination nearby equilibrium: kinetics, CaO crystal structure, sintering and reactivity, J. Phys. Chem. C 119 (4) (2015) 1623–1641.
[30] E. Fundal, The burnability of cement raw mixes, World Cem. Technol. (1979) 195–204.
[31] D.H. Campbell, C.T. Laboratories, *Microscopical Examination and Interpretation of Portland Cement and Clinker*. 1986: Construction Technology Laboratories.